Cosmic-Ray Interactions at 10^{11}–10^{13} eV*

E. W. Cowan and K. Matthews
Physics Department, California Institute of Technology, Pasadena, California 91109
(Received 12 April 1971)

A sample of 1167 single cosmic rays near sea level is analyzed from the data recorded by an interleaved stack of cloud and ionization chambers, and carbon and iron plates. The results include loss-rate curves in iron and carbon, mean free path in carbon, and energy spectra of charged hadrons (largely pions) and neutrons.

INTRODUCTION

An ion-chamber cloud-chamber array of overall dimensions 5.8 m by 1.6 m by 0.9 m has been operated at 250 m above sea level to investigate cosmic-ray interactions at high energies. Some of the characteristics of the individual cloud and ion chambers have been previously described.[1] A front view showing the general layout is in Fig. 1, with a typical shower drawn as it would appear in one of the stereoscopic photographs that also record the readings of the eight flat ion chambers. A side view would be similar with horizontal dimensions decreased by a factor of about 0.6.

Photographs were taken whenever the total energy absorbed in the iron, as sampled by the ion chambers, exceeded a trigger level of about 140 GeV, which occurred about three times per hour. The 22 000 pictures obtained in 0.85 year of sensitive time were later sorted to remove all containing more than one parallel track, since the proportion of the ion-chamber readings to be attributed to different simultaneous particles observed was unknown. The most energetic single strongly interacting particle observed measured 7400 GeV. The presence of a core of particles in the cloud chambers within the ion-chamber stack, together with the hodoscope display above the ion chambers, helped correlate a single incoming particle with the energy measurement. A total of 1167 single particles within a solid angle area of 0.65 sr m^2, defined by rectangular windows within the gas of cloud-chamber 6 and ion-chamber 4, form the basis of most of the following results.

PARTICLE IDENTIFICATION

The separation of charged from neutral incoming particles was made using the part of the photographs showing the upper cloud-chamber stack. Particles were eliminated if an interaction occurred before the charge could be determined within the fiducial volume. The remaining sample contained 977 particles that passed through at least one cloud-chamber window before interacting. Sixteen electrons and nine γ rays were identified from the characteristic loss-rate curves of the electronic shower cascade in the iron of the calorimeter. Muons also give rise to electronic cascades, starting within the calorimeter rather than at the top, and 78 such particles were identified by this means and, in addition in some cases, by the appearance of the penetrating muon in the cloud chambers within the calorimeter.

The electrons have a broad zenith-angle distribution similar to that of the muons, and presumably arise from the decay of muons close enough to the apparatus for electronic multiplication not to have occurred. Within the limitation of the small number of γ rays observed, the γ-ray zenith-angular distribution and energy spectrum are the same as for the hadrons. The number of γ rays is in rough agreement with the number expected from the decay of neutral pions at a distance large enough that the separation of the two γ rays results in only one entering the apparatus but small enough that no electron shower is started in the air. The remaining particles in the sample consist of 890 strongly interacting particles (hadrons).

Measurement of the neutral/charge ratio requires that both types of particles be selected on a similar basis, and since the identification of neutral particles requires an interaction above the calorimeter, charged particles were similarly selected. The observed ratio also involves the relative interaction lengths of the two types of particles. A further requirement, that the line of flight of all particles pass through about two interaction lengths above the calorimeter, reduces this effect and gives for particles of average energy 330 GeV a ratio of neutral/charge = 90/305 = 0.295 $\pm$ 0.035, where the error is the standard deviation from statistical effects only. A value greater than 0.4 is expected from measurements at higher altitudes extrapolated to sea level with the assumption that pion-nucleon collisions are inelastic.[2,3] If the interaction length of neutral particles were to be twice that of charged particles, this would give

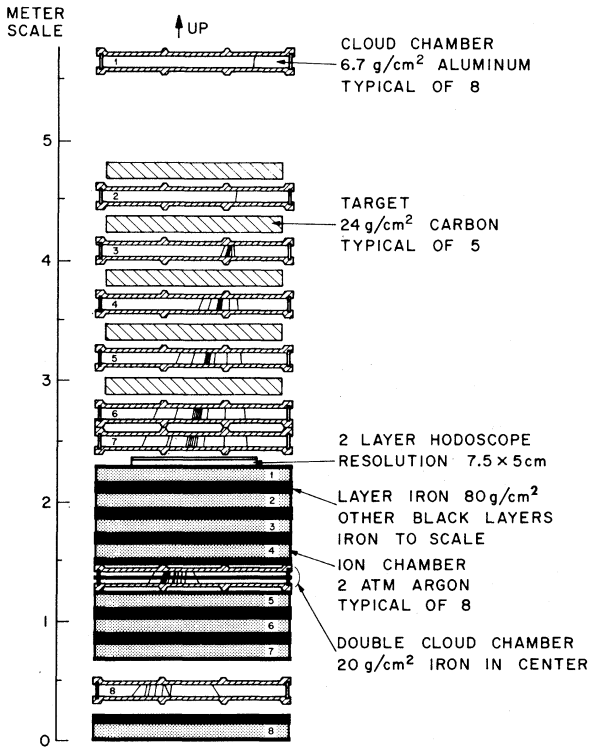

FIG. 1. Over-all layout of cloud-chamber ion-chamber stack. Total material below the hodoscope is 630 g/cm^2. The side view is similar with horizontal dimensions multiplied by 0.6.

approximate agreement, but no such difference is indicated by the results presented in a later section.

A different apparatus consisting of a large multiplate cloud chamber containing 11 iron plates totaling 254 g/cm^2 has also been used to measure neutral/charge = 155/636 = 0.244 at the same elevation of 250 m above sea level. Here interactions in the iron plates were used to identify hadrons of energy greater than 50 GeV. This sample included associated incoming particles with small separation.

Calculations[2,4] of the neutron/proton ratio give a value greater than 0.9 at sea level. Although this value has not been measured directly at sea level for energies above 100 GeV,[5] numerous measurements[2,3,6,7] of neutral/charge at high altitude give a lower limit for neutron/proton around 0.7, and this would be expected to increase at lower depths in the atmosphere. Assuming neutrons/protons = 0.9, the present sample of charged particles corresponds to pions/protons = 2.05. Comparison of the neutral and charged particles is therefore largely a comparison of neutrons and pions.

It should be noted that the measured neutral/charged ratio depends on the area over which an accompanying particle is forbidden. The extent to which this differs from the true ratio depends on the detailed evolution of the atmospheric showers containing the particles. The comparison of results from different apparatus at different altitudes is thus somewhat indirect. The multiplate chamber, which accepts closely spaced hadrons, gives a neutral/charged ratio largely independent of previous interactions in the atmosphere. In the present experiment more charged pions than protons may be eliminated if the last interaction of the pions in the air is lower on the average than that of the protons. Other effects also enter. A proton of a given energy emerging from an interaction in air will in general be surrounded by particles of a different angular distribution and composition than those surrounding a pion of the same energy. A measurement of the pion/proton ratio in a lower energy range[5] appears to extrapolate to a much lower value than that obtained here. Although the conclusion of a neutron/proton ratio near unity at sea level seems difficult to escape, a direct measurement of this ratio would be valuable since the other measurements to be reported furnish no indication of the relative proportion of pions.

ENERGY-LOSS-RATE CURVES

The rate of energy loss divided by energy for charged hadrons is shown in the scatter plot in Fig. 2, which shows the individual measurements of each ion chamber plotted in energy bins at the correct range in g/cm^2 from the interaction. This sample includes 291 particles of average energy 320 GeV that interact in light material in the cloud-chamber fiducial volume, which gives an accurate location for the interaction. The range is corrected for factors such as ribs and walls of the cloud chambers and the tilt of the track. The scatter in the points represents real fluctuations in elasticity, multiplicity, and the distance between secondary interactions that occur for each particle. The average loss rates for each range bin from such scatter plots are shown in Fig. 3 for 76 neutral and 291 charged hadrons that interact within the cloud-chamber fiducial volume. A change of slope near 400 g/cm^2, appears in both of these curves and also in the curves (not shown) of a second independent sample containing 46 neutral and 156 charged particles. This change, which is not the result of a miscalibrated ion chamber, is near the range where the light material of the double cloud chamber is inserted in the calorimeter.

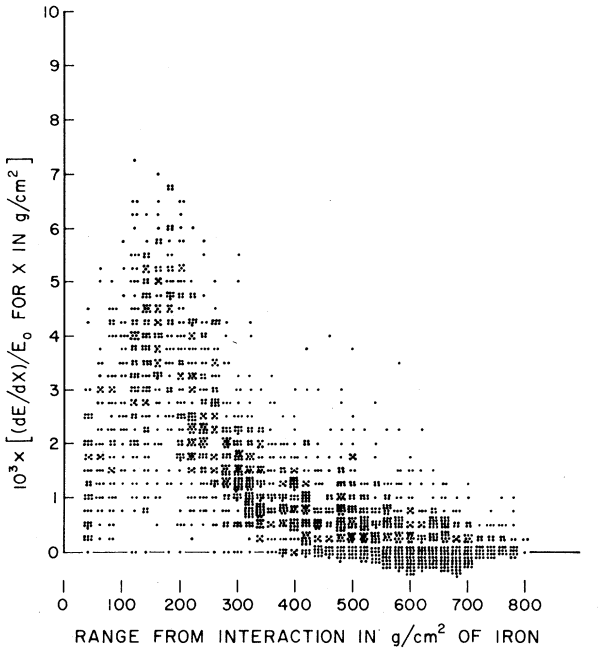

FIG. 2. Rate of loss of energy in iron per unit primary energy for 291 charged hadrons of average energy 320 GeV. The points below the horizontal axis represent a measurement of zero.

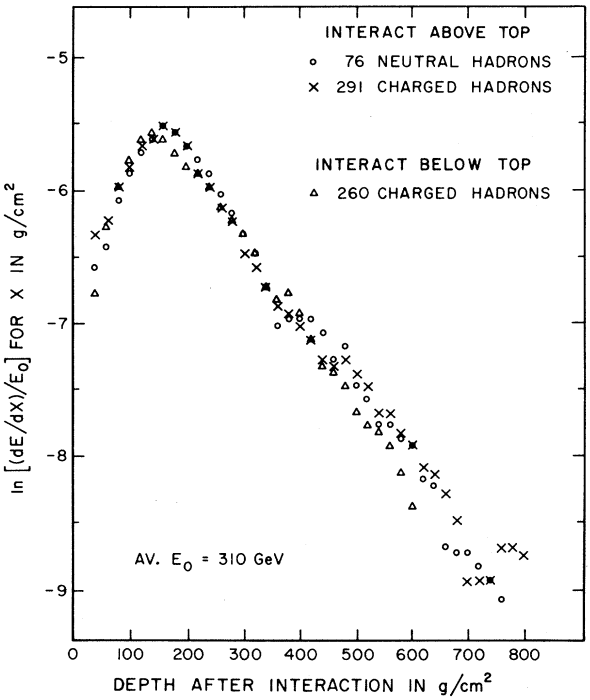

FIG. 3. Average rate of energy loss per unit primary energy in iron of the shower products of charged and neutral hadrons. Each curve has been smoothed by a three-bin average. Initial interactions above top are in carbon or aluminum; those below the top are in iron.

Points for a similar loss-rate curve are also shown in Fig. 3 for 260 charged hadrons that have their first interaction in the iron of the calorimeter. The interaction point is determined by an extrapolation of the average energy loss-rate curve, which involves systematic errors of the order of the size of the 20-g/cm^2 range bins. The fact that the initial interaction is in iron rather than carbon or aluminum causes no appreciable change after the initial rise in the curve.

Within statistical errors, the curves for neutral and charged hadrons are identical, indicating that the secondaries from cascades in iron initiated by pions or by nucleons lose energy at the same rate. This result, which appears true for all energies considered, is consistent with a high inelasticity for both the pion-iron-nucleus and nucleon-iron-nucleus interactions.

For comparison with calculations,[8] curves similar to those in Fig. 3, with loss rate as a function of distance from the interaction, have been folded with the probability of the primary particle interacting at a given depth in the iron calorimeter. The resulting loss rates are plotted in Fig. 4 as a function of depth in the iron for assumed interaction lengths $L = 120$ g/cm^2 and $L = 160$ g/cm^2. This includes most of the measured values.[9-13] Comparison of these curves with those of Pinkau and Thompson[8] gives agreement for inelasticities K between 0.6 and 1.0, the larger values of K corresponding to larger L.

All of the energy-loss-rate curves plot $(dE/dx)/E_0$, the energy-loss rate divided by the energy of the primary particle E_0. In this form, curves such as those in Figs. 3 and 4 are nearly independent of E_0. There is a small tendency apparent in the sets of curves for different energies in Fig. 4, for the curves to be higher at larger depths for high energies. That is, high-energy particles lose a slightly greater proportion of their total energies at greater depths in the target. However, within the range $10^{11}-10^{13}$ eV, the curve of Fig. 3 is a fairly good universal curve, applying to both neutral and charged particles. An average attenuation length of 169 g/cm^2 has been used to describe the approximately straight part of the curve to calculate the energy lost after the particle passes through the last ion-chamber window. The average of this correction is 4.5% for all of the hadrons interacting in the cloud-chamber fiducial volume, and 8.7% for those interacting below this volume. The total energy E_0 of the incoming particles has been obtained by adding the energy sampled by the ion chambers, the correction for the energy lost out the botton, and the energy lost in the carbon and aluminum targets estimated by counting

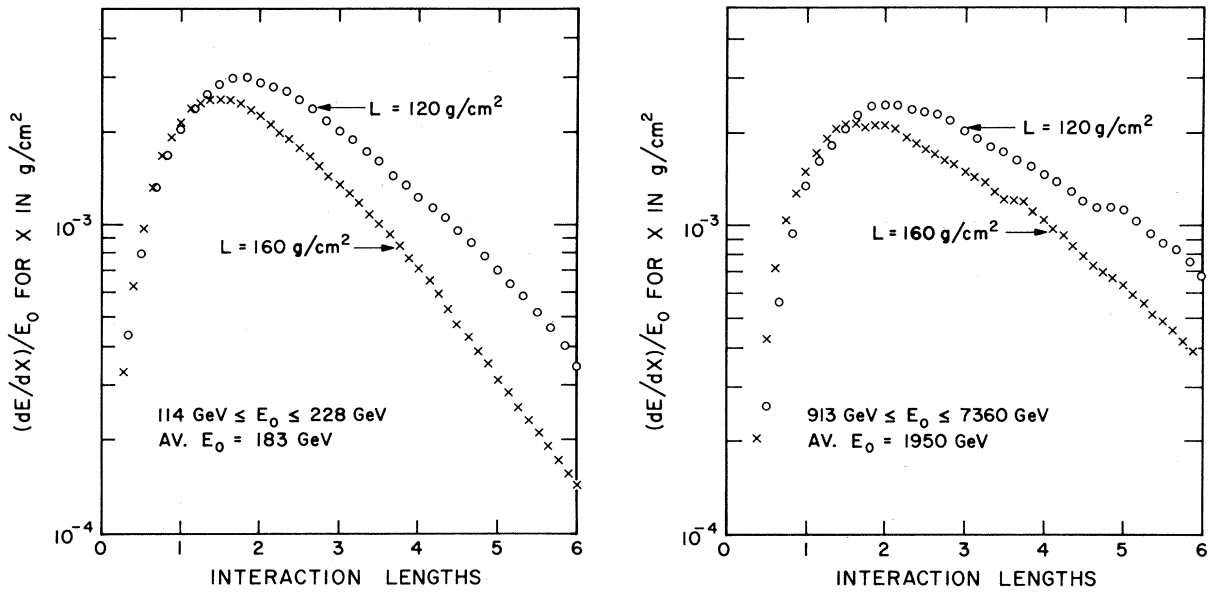

FIG. 4. Average rate of energy loss per unit primary energy in iron target of the shower products of hadrons in the energy ranges shown. These curves are produced by folding curves similar to Fig. 3 with a probability function corresponding to the first interaction after a mean free path L.

tracks in the cloud chambers. The energy lost in slow neutrons, neutrinos, and nuclear binding energy, which is not measured by the ion chambers, has been estimated[14] at 6% at 300 GeV, decreasing at higher energy. A correction for this has not been made in any of the data, and it is unimportant except where noted in the section on energy spectra.

The curve in Fig. 3 has also been used to predict the readings of the calorimeter if the interaction point were to be moved up along the path of the particle to its entrance point in the apparatus. This is essential for the sampling bias correction used in the mean-free-path analysis in a later section.

It might be expected that loss rates in lighter elements, where the inelasticity is less, would show up differences between the pions and nucleons. Figure 5 shows similar loss-rate curves made for the targets in the top part of the stack, which are mostly carbon, comparing charged and neutral particles in each of two energy ranges. The points on these curves represent the loss rate deduced from the number, density, and length of tracks counted visually from the photograph of the interaction cascade developing in the cloud chambers. The number of tracks in the dense parts of the shower could only be estimated in many cases where individual tracks could not be resolved, but the resulting errors should have little systematic relation to whether the primary causing the event is charged or neutral. A difference in the angular distribution of secondaries could produce

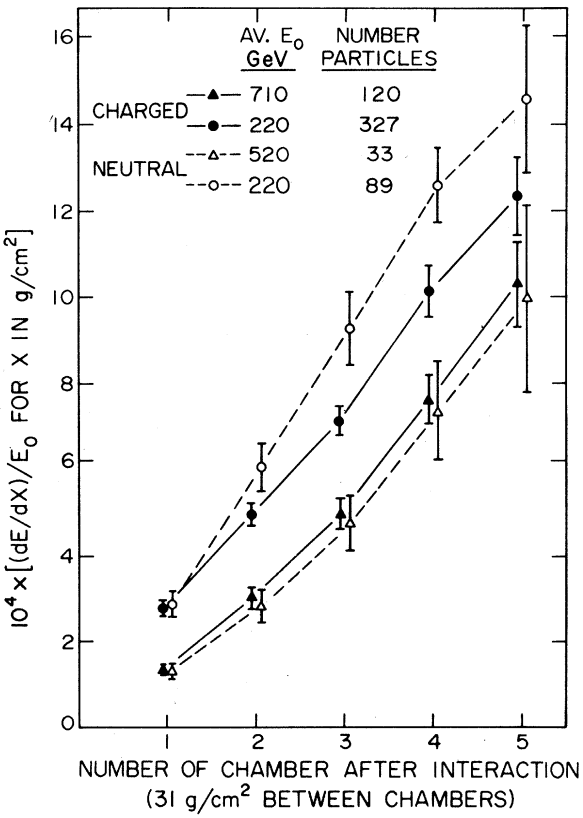

FIG. 5. Average rate of energy loss of the shower products of charged and neutral hadrons in carbon and aluminum target plate per unit primary energy.

some systematic difference. It should be noted that the errors indicated by the standard deviation at each point are correlated for successive points along a given curve. A sample of primary particles that happens to have a high average count of secondaries at a given chamber because of a statistical fluctuation will also tend to have a high count in chambers thereafter. The confidence in one curve being above another is more nearly related to the error at a single point than to the entire curve.

These curves again show negligible difference between the neutral and charged interactions, with possibly a slightly higher average track count at lower energies from the showers with neutral primaries. The inelasticity for carbon nucleus interactions appear not much different for neutral and charged primaries. There is thus no appreciable effect on the loss-rate curves in carbon and iron as a result of differences in the nucleon-nucleon and pion-nucleon average inelasticity within the range of this experiment.

MEAN FREE PATH

The geometry in the upper part of the cloud-chamber ion-chamber stack consists essentially of five thin targets interleaved with cloud chambers. Each target consists of 24 g/cm^2 of carbon together with 5.7 g/cm^2 of aluminum and 1 g/cm^2 steel in the walls of the cloud chambers. A maximum-likelihood procedure has been used to find the mean free paths of hadrons in the targets, which were treated simply as uniform plates of mass 30.7 g/cm^2.

The location of the interaction along the portion of a track within the cloud-chamber fiducial volume was used in the likelihood procedure to predict the probability of observing the given sample of photographs as a function of an assumed mean free path M. This probability was then maximized by varying M. Although the interaction location can be determined by extrapolating the shower tracks into the target plates, there is a small systematic error downward. The large sensitivity of the likelihood procedure to this type of systematic error requires the following procedure that uses only the location number of the plate of interaction, which can be determined with certainty in all but a few cases. An analysis generalized to plates of different materials permits the inclusion of the calorimeter as one of the target plates. Allowance can then be made for particles above the bias energy that do not interact high enough in the calorimeter to deposit a sufficient fraction of their energy for a trigger.

The probability π_n of passing through a succession of n plates without interacting is the product of $p_0 = 1$ times the n probabilities $p_j = e^{-m_j/M_j}$ for not interacting in each plate, where the jth plate has thickness m_j and material of mean free path M_j. Given a random sample S of particles whose paths go through N plates and the subset S_1 of particles that interact at least once, the following relation holds. The probability C that a particle in S shows a first interaction in plate n equals the probability π_{n-1} of reaching plate n without interacting multiplied by the probability $1 - p_n$ of interacting in plate n. The probability C also equals the probability $1 - \pi_N$ that a particle in S will be in the subset S_1 multiplied by the probability P_i that a random particle i from S_1 will show an interaction in plate n. The probability P_i is obtained by equating the two expressions for C:

$$P_i = \pi_{n-1}(1 - p_n)/(1 - \pi_N).$$

The product of the separate P_i for the set of particles observed to interact in the plates is the likelihood function P, which is the probability of obtaining this set by drawing from a random set of interacting particles. In the limit of small m_j, this becomes the conventional likelihood function for a continuous distribution of interaction points. The "random" set of particles is assumed to be made up from a large number of pictures of particle tracks along each of the lines actually observed, but random with respect to interactions along these lines. The values of m_j and N can thus be given individually for each picture, permitting the use of particles which have oblique incidence or which miss some of the plates. The thickness m_j assigned to the calorimeter considered as a target plate is not the total mass along the path of the particle but that portion of the mass before the last point at which an interaction will cause the sum of the ion-chamber pulses to exceed the trigger level. This is computed for each picture using the loss-rate curves previously discussed. The values of the mean free paths M_j that maximize P are the most likely values in the absence of any other information, and the shape of P as a function of M_j gives the relative probability of other values. Only the mean free path M in the five thin target plates is varied in the curves in Figs. 6 and 7, since the maxima of these curves shift only a few percent in M as the mean free path in iron is varied from the value used of 130 g/cm^2 to zero. Since only relative values of P are of interest, all curves are plotted with a peak value of unity.

A sampling bias in the original sample of 890 hadrons must be removed before using the likelihood procedure. This bias is introduced by the calorimeter trigger level, regardless of whether this rejection limit is imposed by the apparatus

or after the interaction photographs have been selected, and regardless of whether the mean free path is a function of energy. Essentially, the bias occurs because the ion chambers sample only part of the energy lost in the apparatus, and the position of the sample on the loss-rate curve depends on the position of the interaction in the target. A particle interacting low in the target may trigger the apparatus, whereas the same particle interacting higher would not. This type of bias must also be avoided when placing the particles in energy bins.

The energy sampling bias has been eliminated by predicting from the average energy-loss-rate curves the readings of the ion chambers if the interaction point were to be moved to the point where the particle enters the cloud-chamber fiducial volume. A picture is retained only if the total of these predicted ion-chamber readings E_p is above the apparatus trigger level E_b plus a small bias margin E_m to allow for fluctuations in the energy-loss rate of the particle. Particles that interact too late in the calorimeter do not trigger the apparatus, but this has already been taken into account in the definition of the m_j for the calorimeter. A picture meeting the sampling bias condition would thus be included in S_1 regardless of where the interaction occurs on the path through the targets. This is the assumption made in the likelihood procedure. The three curves in Fig. 6 marked P_2, which include all charged hadrons regardless of whether or not they interact in the cloud-chamber fiducial volume, show the effect of this bias correction. These curves represent the likelihood functions with no sampling bias correction and with E_m equal to 0 and 28 GeV.

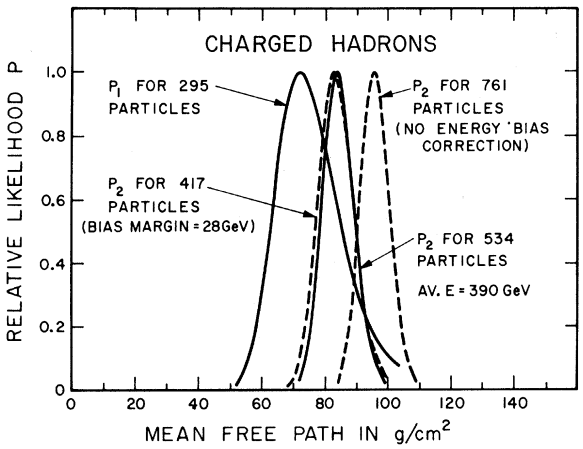

FIG. 6. Likelihood functions for mean free path of charged hadrons. Dashed curves show effect of sampling bias correction discussed in text. Bias margin is zero for solid curves.

Since increasing E_m above zero broadens the curves with little systematic shift in the maxima, $E_m = 0$ has been used for all of the curves in Figs. 6 and 7 where not otherwise indicated.

After the bias correction, the likelihood curve corresponds to a mean free path of 84 ± 6 g/cm^2. This corresponds to an average cross section of 272 ± 19 mb for target nuclei. If the cross section for the target materials other than carbon is weighted in atomic number as $A^{2/3}$, the carbon-nucleus cross section is 252 ± 18 mb. The criterion for determining what is an "interaction" has been to require that the primary particle emerge from a plate accompanied by a penetrating particle visible in at least two cloud chambers after the interaction. A single recoil proton with an energy sufficient to penetrate 60 g/cm^2 would have been counted as an interaction, although no interactions this marginal were found. A cross section deduced from the above mean free path is therefore close to a total cross section.

The curves in Fig. 7 show the likelihood curves P_2 for charged particles divided into three energy bins, using the corrected energy E_0 to avoid the bias just discussed. No significant change in mean free path is apparent in this energy range. When an assumed linear dependence of M on energy E is included in the maximum-likelihood analysis in the form $M = M_0 - AE$, where E is in GeV, the value $A = 4.2 \times 10^{-3}$ g cm^{-2} GeV^{-1} for maximum likelihood is only 18% more probable than $A = 0$.

The likelihood curves designated P_2 are calculated from a subset S_1 in the likelihood procedure that includes the calorimeter as a target plate, regardless of whether the particles show interactions in the cloud-chamber fiducial volume.

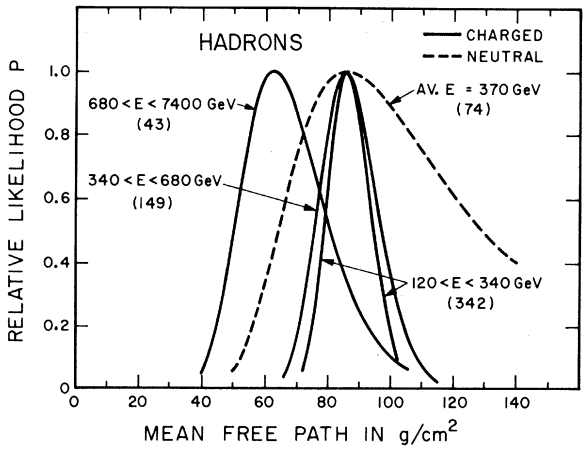

FIG. 7. Likelihood functions for mean free path of charged and neutral hadrons of various energies. Average energies of the charged particles in each of the three energy bins are 240, 470, and 1320 GeV. The number of particles in sample is in parentheses.

Another likelihood curve P_1 is obtained by restricting the subset S_1 to those pictures that contain an interaction in the cloud-chamber fiducial volume. Only this method is possible for neutral particles since a diffuse shower core in the double cloud chamber in the calorimeter does not accurately determine the line of the flight through the upper cloud-chamber fiducial volume. The likelihood P_1 avoids any possible scanning bias for missing energetic particles that have no interaction in the fiducial volume, which is possible for P_2, but P_1 has a much greater sensitivity to the energy sampling bias correction. Without this correction, the maximum of P_1 shifts to infinity. However, with this correction, the curves of P_1 and P_2 in Fig. 6 for charged hadrons are in reasonable agreement, and the dashed curve in Fig. 7 of P_1 for neutral hadrons permits a comparison of neutrons and charged particles that are mostly pions.

ENERGY SPECTRA

The integral energy spectra of 94 neutral and 350 charged hadrons interacting in the cloud-chamber fiducial volume are compared in Fig. 8. The vertical coordinate of each point represents the number of particles with energy greater than E_0 divided by the aperture, 0.65 sr m^2, and by the operating time for which the apparatus was sensitive to all energies deposited in the calorimeter greater than $(E_0 - 5.7\ \text{GeV})/1.2$. Each point differs from its neighbors by one event. The energy trigger allowance ensured that the apparatus was sensitive to all particles of energy E_0. Within the

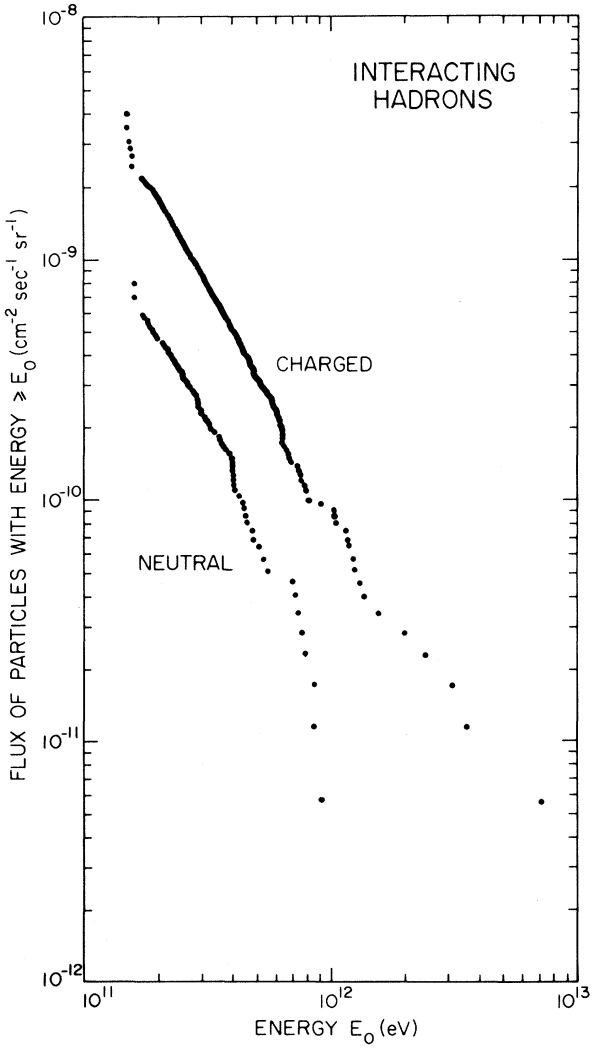

FIG. 8. Integral energy spectrum of interacting charged and neutral hadrons.

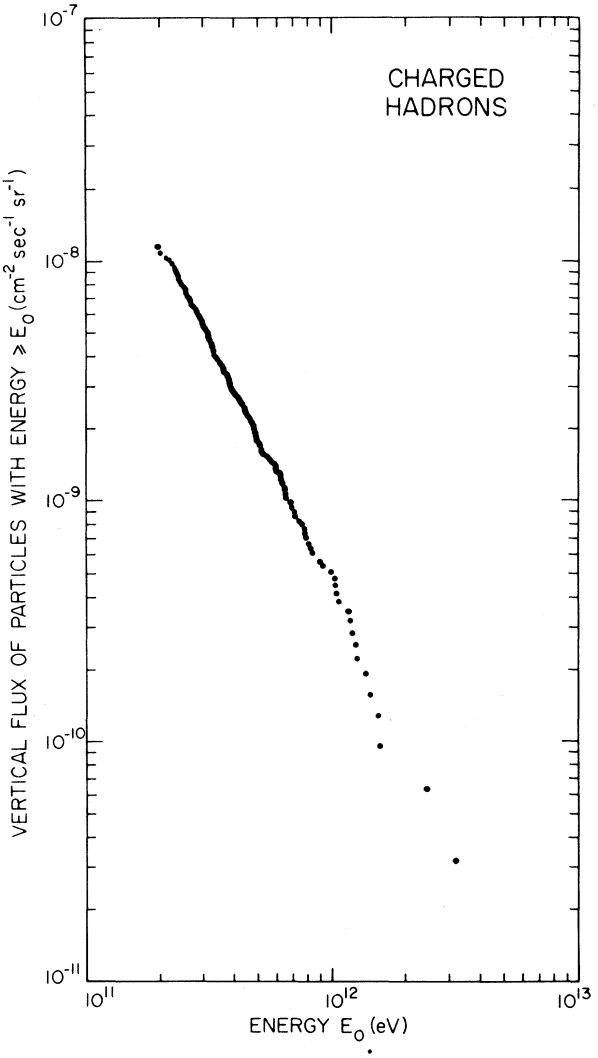

FIG. 9. Integral energy spectrum of charged hadrons corrected to absolute vertical flux.

statistical errors, the slopes of the two spectra are the same. The relative numbers of the neutral and charged particles represent only approximately the true relative fluxes since the requirement of an interaction in the fiducial volume involves the relative interaction lengths.

A plot of the absolute vertical flux obtained from charged hadrons selected without the requirement of an interaction in the fiducial volume is in Fig. 9. The trigger allowance has been increased to $(E_0 - 5.7\ \text{GeV})/1.5$, and the curve is normalized to read the absolute flux extrapolated in angle to the vertical. Passage of the line of flight of the particle through the first seven ion-chambers windows was required to minimize the correction for the loss of particles that interact too late in the calorimeter to exceed the trigger level. A small correction was also included for 3.5 g/cm^2 of aluminum above the target fiducial volume. For charged hadrons of energy greater than 227 GeV, the vertical flux is $(1.01 \pm 0.09) \times 10^{-8}$ cm^{-2} sec^{-1} sr^{-1}, where the error is the standard deviation calculated from the number of particles. The error in the energy 227 GeV is also important because of the steepness of the spectrum, which has a slope of 2.11 ± 0.12. A correction of the order of 6% (Ref. 14) should be added to the energy 227 GeV for losses absorbed by nuclear binding energy in the calorimeter. This correction decreases with increasing energy in an unknown manner. With the correction, the curve would have a slightly steeper slope. The requirement that we used, of no accompanying particle, steepens the slope by biasing against high-energy particles. A systemic error of the order of 5% is possible in the absolute calibration of the calorimeter from uncertainties in the ratio of loss rates of the shower particles in 2-atmosphere argon and iron. The shower particles were assumed to be electrons at the critical energy in iron. The electrical calibration was within 5%.

The arrival directions in astronomical coordinates of the high-energy particles are determined by the tracks in the cloud chambers with errors of the order of 0.1°. No anisotropy in right ascension is observed and none would be expected for charged primaries in this energy range. The directions of 1201 particles have been checked against the directions of supernovas and other unusual astronomical objects for a coincidence within 0.1°, indicating a possible point source of neutral particles. The results were negative and will not be reported in detail since rough calculations show negligible chance of observing the neutrons that might be expected from such objects. The neutrons would result from the photodissociation of high-energy nuclei[15,16] by photons from the same source.[17] A large shower detector with comparable angular accuracy might have some chance of success in the period shortly after a supernova since there should be an appreciable flux of neutrons of energy high enough to travel across the galaxy before decaying.

ACKNOWLEDGMENTS

It is a pleasure to acknowledge the advice and encouragement of Professor C. D. Anderson in these experiments and the assistance of Willem Bury in the maintenance and operation of the equipment.

---

*Work supported in part by the U. S. Office of Naval Research under Contract No. Nonr-220 (53).

[1]E. W. Cowan and M. K. Moe, Rev. Sci. Instr. 38, 874 (1967).

[2]Y. Pal and B. Peters, Kgl. Danske Videnskab. Selskab, Mat.-Fys. Medd. 33, No. 15 (1964).

[3]V. V. Avadkian and M. P. Pleshko, Can. J. Phys. 46, S709 (1968).

[4]S. Hayakawa, *Cosmic Ray Physics* (Wiley, New York, 1969), p. 342.

[5]G. Brooke, M. A. Meyers, and A. W. Wolfendale, Proc. Phys. Soc. (London) 83, 871 (1964).

[6]L. W. Jones, A. E. Bussian, G. D. DeMeester, B. W. Loo, D. E. Lyon, Jr., P. V. Ramana Murthy, R. F. Roth, J. G. Learned, F. E. Mills, D. D. Reeder, K. N. Erickson, and Bruce Cork, Phys. Rev. Letters 25, 1679 (1970); 26, 213(E) (1971).

[7]S. Lal, Y. Pal, and R. Raghaven, J. Phys. Soc. Japan 17, Suppl. A-III, 393 (1962).

[8]K. Pinkau and K. V. Thompson, Rev. Sci. Instr. 37, 302 (1966).

[9]E. L. Andronikashvili, L. L. Gabuniya, D. I. Garibashvili, D. B. Kakauridze, D. M. Kotylarevskii, Z. Sh. Mandzhavidze, L. A. Razdol'skaya, N. M. Roinishvili, N. G. Talalashvili, G. E. Chikovani, L. D. Chikovani, and E. N. Sherer, Bull. Acad. Sci. USSR, Phys. Ser. 32, 364 (1968). [See also E. L. Andronikashvili, G. E. Chikovani, D. I. Garibashvili, L. L. Gabunia, D. B. Kakauridze, D. M. Kotlyarevski, Z. Sh. Manjavidze, N. N. Roinishvili, L. A. Razdolskaya, and E. N. Sherer, Can. J. Phys. 46, S689 (1968).]

[10]V. V. Guseva, E. V. Denisov, N. A. Dobrotin, N. G. Zelevinskaya, K. A. Kotel'nikov, A. M. Lebedev, V. M. Maksimenko, A. E. Morozvo, and S. A. Slavantinskii, Bull. Acad. Sci. USSR, Phys. Ser. 33, 1299 (1969).

[11]A. E. Brenner and R. W. Williams, Phys. Rev. 106, 1020 (1957).

[12]D. I. Garibashvili and D. B. Kakauridze, Bull. Acad. Sci. USSR, Phys. Ser. 31, 1495 (1967).

[13]E. V. Denisov, Bull. Acad. Sci. USSR, Phys. Ser. 32, 366 (1968).

[14]V. S. Murzin, Progr. Elem. Particle Cosmic Ray Phys.

9, 291 (1967).
[15]J. P. Ostriker and J. E. Gunn, Astrophys. J. 157, 1395 (1969).
[16]J. E. Gunn and J. P. Ostriker, Phys. Rev. Letters 22, 728 (1969).
[17]J. B. Pollack and B. S. P. Shen, Phys. Rev. Letters 23, 1358 (1969).

PHYSICAL REVIEW D VOLUME 4, NUMBER 1 1 JULY 1971

Backward-Angle Electron-Proton Elastic Scattering and Proton Electromagnetic Form Factors*

L. E. Price,† J. R. Dunning, Jr.,‡ M. Goitein,§ K. Hanson, ‖ T. Kirk, and Richard Wilson

Harvard University, Cambridge, Massachusetts 02138
(Received 8 February 1971)

Elastic electron-proton scattering cross sections were measured at backward angles (80°–90°) in the laboratory for four-momentum transfers between 7 F^{-2} and 45 F^{-2}. Experimental errors range from 3.1% to 5.3%, including a systematic error estimated to be 1.9% added in quadrature. Electric and magnetic form factors are computed from all the recent data in this q^2 range, with allowance made for possible normalization differences. The results show a deviation from the scaling law.

I. INTRODUCTION

We report here on the second part of a program of measurements of elastic electron-proton scattering, designed to permit form-factor separation. The earlier experiment[1] measured forward-angle scattering. We report now on the measurements of backward angles. The kinematic conditions of our data points are summarized in Table I.

II. APPARATUS

The apparatus used to scatter the electrons and detect the results is shown schematically in Fig. 1. Electrons from the Cambridge Electron Accelerator (CEA) are directed at a liquid hydrogen target. Electrons scattered at large laboratory angles (usually 90°) in the horizontal plane enter the spectrometer and are momentum analyzed. The recoiling protons are detected by a scintillation counter telescope. Unscattered electrons continue on to two beam-monitoring devices, a secondary emission monitor (SEM), and a Faraday cup.

The concept of the measurement, and even certain pieces of equipment, were identical with the forward-angle measurement of Ref. 1. We comment here on the differences that were necessary in order to measure backward-angle scattering.

(1) Every effort was made to increase the solid angle of the electron spectrometer as much as possible. Thus a full quadrupole magnet was used in the electron spectrometer instead of the half-quadrupole, used previously. Also the magnet and counters were placed closer to the target.

(2) The electron solid angle was defined in two places. The vertical angle was defined by an aperture A_1 consisting of 0.5 in. of tungsten before the quadrupole. Separate apertures allowed scattered electrons to enter the upper and lower half of the magnet. The horizontal angle was defined after the quadrupole by scintillation counters S_L and S_R on either side of a lead aperture 4 in. thick. Each counter overlapped the aperture A_2 by 0.1 in. The fraction of the scattered particles seen by each counter agreed with calculation within the statistical error of 0.1% of the total. For some runs, in fact, S_L was not working, and it was necessary to rely on the lead aperture A_2 for angular definition on that side.

A Monte Carlo calculation was used to estimate the increase in solid angle from penetration and scattering off the apertures. It was estimated to be $(0.2 \pm 0.1)\%$.

Because the angular definition was done in two different places, the solid angle varied with the scattered momentum. At the center of the spectrometer it was 8.4 msr (for the nominal incident beam position).

(3) The array of slat counters C_1–C_{16}, with edges in the central plane of the quadrupole, which were used to determine the momentum of scattered particles, differed in detail from the one used in Ref. 1. The layout used in this experiment is shown in Fig. 2. The counters were spaced a constant 2 in. apart, giving momentum bins approximately 2% wide. The procedure for determining momentum from the pattern of counter firings is